

# Near-field enhancement by waveguide-plasmon polaritons in a nonlocal metasurface

Xiaorun Zang and Andriy Shevchenko

Department of Applied Physics, Aalto University, P.O. Box 13500, FI-00076 Aalto, Finland

E-mail: [xiaorun.zang@aalto.fi](mailto:xiaorun.zang@aalto.fi)

**Abstract.** Localized surface plasmons in metal nanoparticles are widely used in nano-optics to confine and enhance optical fields. It has been previously shown that, if the nanoparticles are distributed periodically, an additional enhancement can be achieved by coupling the localized surface plasmons to the diffraction orders of the lattice, forming surface lattice resonances. In this work, we study an even further improvement of the near-field enhancement by placing a metal-dielectric slab waveguide beneath the lattice of the particles to excite coupled waveguide-plasmon polaritons. These excitations can extend over many periods of the lattice, making the metasurface highly nonlocal. We numerically demonstrate that the approach can provide a significant extra increase in the near-field intensity – by a factor of 80 over that produced by a single-particle plasmon resonance and by 7 over the lattice-resonance enhancement. The described enhancement mechanism can be used to design extraordinarily efficient nonlocal optical metasurfaces for many applications, including surface-enhanced Raman spectroscopy, fluorescence spectroscopy, nonlinear optics, and solar energy harvesting.

*Keywords:* Metasurfaces, Waveguide-plasmon polaritons, Surface plasmons, Bloch wave, SERS, Plasmonics, Field enhancement

## 1. Introduction

Local enhancement of optical fields plays an essential role in many applications of optics and photonics, including optical sensors and detectors [1, 2], light sources [3–6], photovoltaic devices [7–9], and nonlinear optical components [10–12]. An efficient near-field enhancement can be obtained with the help of metal nanostructures that exhibit localized surface plasmon resonances (LSPRs) [13–15]. Due to a high density of metal electrons, light can be strongly squeezed into subwavelength regions [15]. The squeezing is especially effective near locations of abrupt and small-volume inhomogeneities of the structures, including interparticle gaps and sharp edges. At such inhomogeneities, very high field intensities can be obtained. For example, the optical intensity in the gap of a gold bowtie antenna consisting of two tip-to-tip facing prisms with sharp corners provides a higher enhancement than the analogue dimer of nanodiscs with round surfaces [16, 17]. These "hot spots" are in the core of many applications, for example, in surface-enhanced Raman spectroscopy (SERS) [18, 19]. The electromagnetic enhancement factor of the SERS signal is given by  $\eta_{\text{SERS}} \approx |E/E_0|^4$  [18], where  $E$  and  $E_0$  are, respectively, the total and incident electric fields in the hot spot.

Nanoparticles of various materials, compositions, shapes, sizes, and surrounding dielectric environments have been explored to control the local field intensity [20–22]. In addition to conventional approaches, high-index dielectric nanoparticles have been recently used to resonantly enhance both the electric and magnetic fields while significantly reducing the ohmic losses [23–26]. Plasmonic dimers that exhibit a toroidal dipole resonance have been shown to outperform the conventional disc dimers regarding the field enhancement and third harmonic generation [27]. It has also been shown that, reducing the gap size increases the local field intensity up to a certain limit dictated by quantum effects, such as the effect of electron tunnelling through the gap and nonlocal screening [28–33]. On the other hand, the quantum confinement effect can play a crucial role for plasmonic particles that are smaller than 10 nm in size [28]. Recently, quantum confinement of electrons in a one-dimensional metallic single-walled carbon nanotube with a diameter of 1-2 nm was reported to form a quantized Luttinger-liquid plasmon that exhibits a strong spatial confinement and low attenuation loss. Such quantum plasmons could be useful for plasmonic integrated devices [34].

Much higher local fields can be obtained by arranging plasmonic nanoparticles in a lattice [35, 36] or superlattice [37, 38]. In this case, the field scattered by one particle can arrive at the neighbouring particles in phase with the other scattered fields, when the periods are appropriate [38–40]. This results in collective LSPRs, which have also been called plasmonic surface lattice resonances [38, 41, 42] or collective lattice modes [38–40, 43]. These excitations lead to a further increase in the local field around each nanoparticle. It has been estimated that a surface lattice resonance can increase the local field intensity by an order of magnitude [44–46]. In the case of a superlattice, the field enhancement can be achieved simultaneously at multiple modes [37]. Moreover, LSPRs can be coupled to optical modes guided in the substrate of a planar metasurface [47], leading to the so-called waveguide-plasmon polaritons (WPPs) [48, 49]. It has been shown that a hyperbolic metasurface can support such hybrid waves or quasi-TE and quasi-TM modes [50]. Very recently, an array of lossy plasmonic nanoparticles on a dielectric slab waveguide was shown to guide a resonant mode of hybrid polarization states with an ultrahigh quality factor [51]. WPPs hold great potential for yielding extra near-field enhancement in arrays of plasmonic nanoparticles, and in our opinion, an in-depth investigation into this mechanism is highly relevant and important.

In this work, we design and study a nonlocal metasurface [52] that provides a significant

additional near-field enhancement by WPPs. The metasurface consists of a lattice of silver nanodimers mounted on a metal-dielectric slab waveguide. Besides a gap enhancement in each nanodimer, an additional intensity enhancement – by a factor of 80 – arises from the coupling of LSPRs to the guided Bloch modes. These modes belong to the second stop band of the structure, exhibiting a collective resonance at normal incidence. Metasurfaces of this type can be used for many applications, but for the purpose of demonstration, we consider a SERS substrate operating at a wavelength of 780 nm, one of typical wavelengths in Raman spectroscopy [53]. At this wavelength, the SERS enhancement in each gap of the dimers is more than 6000 times higher than that in an isolated dimer on a semi-infinite dielectric. The metasurface can easily be redesigned to enhance an optical field at any other wavelength. In addition, nonlocal metasurfaces consisting of meta-atoms other than nanodisc dimers, such as bowtie antennae or trimers, are expected to benefit from the extra near-field enhancement by WPPs as well.

The paper is organized as follows. In Section 2, we study the guided modes of a one-dimensional slab waveguide. This study provides a starting point for the design of a planar metasurface and a physical insight into the properties of possible guided Bloch modes. In Section 3, we establish a connection between the near-field enhancement spectra in a designed planar metasurface and the empty-lattice Bloch-mode band diagrams. In Section 4, we optimize the designed metasurface to maximize its near-field enhancement factor. To achieve a significant additional enhancement of light in the gap hot spots, we match the frequencies of the lattice resonances and the guided modes by varying the lattice periods and slab thickness. We draw conclusions in Section 5.

## 2. Guided modes in a slab waveguide

A metasurface considered in this work is composed of a slab waveguide and a lattice of nanoparticles (meta-atoms) on its surface. We first study the properties of the waveguide alone, treating it as a periodic structure with an empty lattice of meta-atoms [40, 54]. A group of qualitatively similar dispersion relations can then be found in a metasurface based on the same slab waveguide [54, 55]. Therefore, it is useful to first investigate the modal dispersion of a slab waveguide and then apply the obtained knowledge to the problem of the near-field enhancement in a real 2D metasurface.

The waveguide is made of a silica slab on a silver substrate [see Fig. 1(a)]. The silver substrate can also enhance the field on the surface by simply reflecting the incident field. The refractive indices of silver, silica, and air are denoted by  $n_{\text{Ag}}$ ,  $n_{\text{SiO}_2}$ , and  $n_{\text{air}}$ , respectively. The dispersive refractive index of silver is downloaded from the online refractiveindex.info database [56], which uses Johnson and Christy's tabulated data [57]. The silica and air regions are treated as having constant refractive indices of 1.4537 and 1, respectively. The waveguide modes are calculated by solving the following one-dimensional problem in a weak formulation, using the finite element method (FEM),

$$\int_C dl \left[ \frac{1}{\alpha} \frac{\partial v_z}{\partial x} \frac{\partial u_z}{\partial x} - \left( \frac{\omega}{c} \right)^2 \gamma v_z u_z \right] = -\beta^2 \int_C dl \frac{1}{\alpha} v_z u_z, \quad (1)$$

where  $u_z$  is the only unknown transverse component of the mode as a function of  $x$ , and  $v_z$  is the corresponding test function. For a TM mode,  $u_z$  denotes the transverse magnetic field and the domain-wise parameters are  $\alpha = \epsilon$  and  $\gamma = \mu$ . For a TE mode,  $u_z$  represents the transverse electric field and the parameters are  $\alpha = \mu$  and  $\gamma = \epsilon$ . The modal propagation constant  $\beta$  is sought by solving the above eigenvalue problem for  $-\beta^2$ . We have implemented the weak formulation calculations using both the Equation-based Module in COMSOL Multiphysics [58] and the open-source software NGSolve [59], which generate consistent results. In the calculations, the semi-infinite

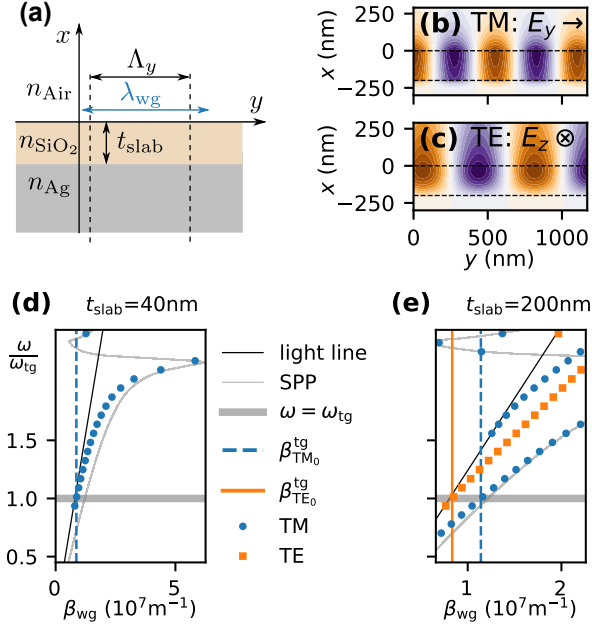


**Figure 1.** (a) A schematic diagram of a silver-silica-air slab waveguide. From top to bottom, the air, silica and silver layers have refractive indices  $n_{\text{air}}$ ,  $n_{\text{SiO}_2}$ , and  $n_{\text{Ag}}$ , respectively. The silica slab layer has a thickness of  $t_{\text{slab}}$ . Field profiles of the fundamental (b) TM and (c) TE modes when the slab thickness is  $t_{\text{slab}} = 200 \text{ nm}$ . The dispersion curves are plotted for (d)  $t_{\text{slab}} = 40 \text{ nm}$  and (e)  $t_{\text{slab}} = 200 \text{ nm}$ . Blue and orange dots indicate the TM and TE modes, respectively. At the target frequency with  $\omega/\omega_{\text{tg}} = 1$ , the propagation constants of the fundamental TM mode  $\beta_{\text{TM}_0}^{\text{tg}}$  and TE mode  $\beta_{\text{TE}_0}^{\text{tg}}$  are indicated, respectively, by vertical blue and orange dashed lines. The black solid line is the light line in vacuum, whereas the grey solid curve plots the SPP dispersion curve at the silver-silica interface.

air and silver regions are truncated by Perfectly Matched Layers (PMLs), which are modelled as frequency-dependent, anisotropic absorbing media [60, 61]. The outside boundaries of PMLs are those of a perfect electric conductor for a TE mode and a perfect magnetic conductor for a TM mode.

The field profiles of the fundamental TM and TE modes are shown in Figs. 1(b) and 1(c), respectively, for a slab thickness of  $t_{\text{slab}} = 200 \text{ nm}$  at the wavelength of 780 nm. The TM mode has a dominant field component  $E_y$  due to the presence of silver at the bottom of the waveguide. It is more concentrated inside the slab and resembles a surface plasmon polariton (SPP) mode at a silver-silica interface [14]. However, the TE mode has only the  $E_z$  component that is nearly negligible at the metal surface and has intensity maxima closer to the silica-air interface. In addition, the TM mode has a shorter modal wavelength than the TE mode, with the former being  $\lambda_{\text{TM}_0} = 550 \text{ nm}$  and the latter being  $\lambda_{\text{TE}_0} = 753 \text{ nm}$ . The modal dispersion curves of slab waveguides with  $t_{\text{slab}} = 40 \text{ nm}$  and  $t_{\text{slab}} = 200 \text{ nm}$  are plotted in Figs. 1(d) and 1(e), respectively. For relatively thin slabs, the fundamental TM mode approximately follows the dispersion curve of the SPP on a silver-silica interface at high frequencies, while it approaches the light line in air at low frequencies. If the slab thickness increases, more modes emerge and the dispersion curve of the fundamental TM mode is

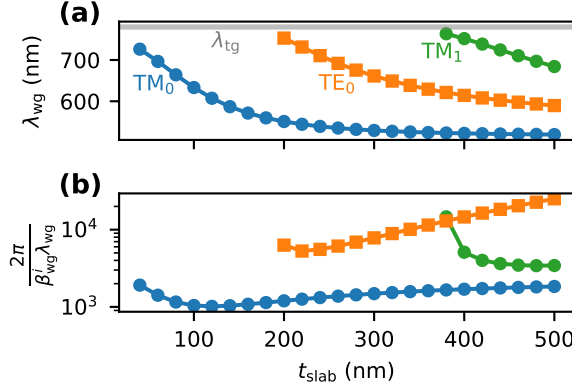


**Figure 2.** (a) Mode wavelengths  $\lambda_{\text{wg}} = 2\pi/\beta_{\text{wg}}^r$  of the slab waveguide; (b) Normalized decay lengths  $2\pi/\beta_{\text{wg}}^i/\lambda_{\text{wg}}$  for a varying slab thickness. The real and imaginary parts of the propagation constant are denoted by  $\beta_{\text{wg}}^r$  and  $\beta_{\text{wg}}^i$ , respectively.

pushed towards the SPP curve. The target wavelength of 780 nm is shown by the horizontal solid grey line that intersects with the dispersion curves and determines the modal propagation constants  $\beta_{\text{TM}_0}^{\text{tg}}$  and  $\beta_{\text{TE}_0}^{\text{tg}}$  at this wavelength.

The wavelengths of the guided modes,  $\lambda_{\text{wg}} = 2\pi/\beta_{\text{wg}}^r$ , with  $\beta_{\text{wg}}^r$  denoting the real part of the propagation constant, are shown in Fig. 2(a) for a varying slab thickness. In addition, the normalized decay lengths,  $2\pi/\beta_{\text{wg}}^i/\lambda_{\text{wg}}$  [62], are plotted in Fig. 2(b), where  $\beta_{\text{wg}}^i$  is the imaginary part of the propagation constant. The guided modes can therefore propagate over a distance of  $10^3$ – $10^4$  modal wavelengths, leading to a long-distance, highly nonlocal interaction of the meta-atoms.

### 3. Bloch modes in plasmonic metasurfaces

Before discussing the guided Bloch modes and lattice resonances in our designed metasurfaces, we extend the empty-lattice dispersion relation of the free-photon approximation [40, 54] to the free-guided-wave approximation. The empty-lattice dispersion relation is

$$|\mathbf{k}_{||} + \mathbf{G}| = \beta_{\text{wg}}, \quad (2)$$

where  $\mathbf{k}_{||} = \hat{y}k_y + \hat{z}k_z$  is the in-plane Bloch wave vector,  $\mathbf{G} = m\frac{2\pi}{\Lambda_y} + n\frac{2\pi}{\Lambda_z}$  is the reciprocal lattice vector (with the integers  $m$  and  $n$  denoting the Bloch-mode orders along the  $y$  and  $z$  directions, respectively), and  $\beta_{\text{wg}}$  is the propagation constant of the slab mode. The slab waveguide is homogeneous and extends to infinity in the transverse plane. However, the fictitious periodicity causes the band folding [40, 54, 55, 63]. If we choose the periods to be equal to the guided-mode wavelengths, the empty-lattice Bloch modes appear to be formed at the  $\Gamma$ -point with  $k_y = k_z = 0$ , which can be used for designing the Bloch modes in a periodic metasurface to be excited at normal incidence [63].

In a metasurface containing silver meta-atoms, the meta-atomic LSPRs are coupled to the empty-lattice Bloch modes, resulting in modified Bloch modes [40]. The unit cell of the metasurface is shown in Fig. 3(a). It contains a meta-atom in the form of a silver-disc dimer with dimensions

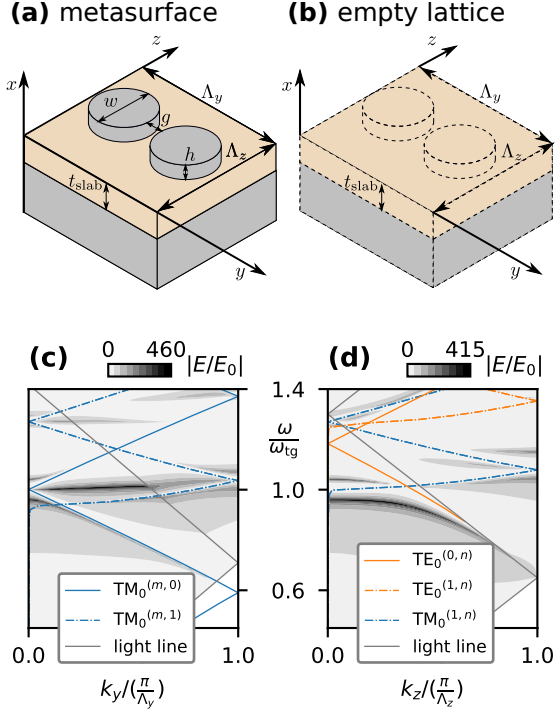


**Figure 3.** Schematic diagrams of (a) a metal-dielectric metasurface and (b) the corresponding empty lattice. The dimer consists of two identical nanodisks with a diameter of  $w$  and a height of  $h$ , which are separated by a gap of  $g$ . The two in-plane periods are  $\Lambda_y$  and  $\Lambda_z$ . In the empty lattice, the dashed outline implies that the nanodisks are actually removed. Note that the dimers in our calculations are about two times smaller than in the pictures. The parameter values used in the calculations are  $\Lambda_y = 550$  nm,  $\Lambda_z = 600$  nm, and  $t_{\text{slab}} = 200$  nm. The near-field enhancement in the metasurface and the empty-lattice dispersion curves are shown in (c) and (d).

$w = 120$  nm,  $h = 20$  nm, and  $g = 6$  nm. The values of other parameters of the structure are  $t_{\text{slab}} = 200$  nm,  $\Lambda_y = 550$  nm, and  $\Lambda_z = 600$  nm. At  $\lambda = 780$  nm, the period  $\Lambda_y$  is equal to the mode wavelength  $\lambda_{\text{TM}_0}$ , but the period  $\Lambda_z$  is shorter than  $\lambda_{\text{TE}_0}$ . Note that plasmonic dimers are among the most efficient standard nanoparticles used to locally enhance optical fields, and dimers composed of nanodisks rather than particles with sharp corners are relatively easy to nanofabricate and treat numerically.

The near-field enhancement spectra in the nonlocal metasurface are calculated using the frequency-domain FEM of the Wave Optics Module of COMSOL Multiphysics [58]. The background excitation field is either a  $p$ - or  $s$ -polarized plane wave in the scattered-field formulation. A  $p$ -polarized incident plane wave (with the electric field lying in the  $xy$ -plane) couples effectively to the TM Bloch modes of the structure, yielding Fano-type [64] asymmetric line shapes in the near-field enhancement spectra. This is revealed in Fig. 3(c), where high (in black) and low (in white) near-field enhancement factors appear near the empty-lattice dispersion curves. A band gap showing low near-field enhancement is formed around the normalized frequency  $\omega/\omega_{\text{tg}} = 1$  at  $k_y = 0$ , as a result of coupling of the LSPR with the empty-lattice Bloch modes  $\text{TM}_0^{(+1,0)}$  and  $\text{TM}_0^{(-1,0)}$  that

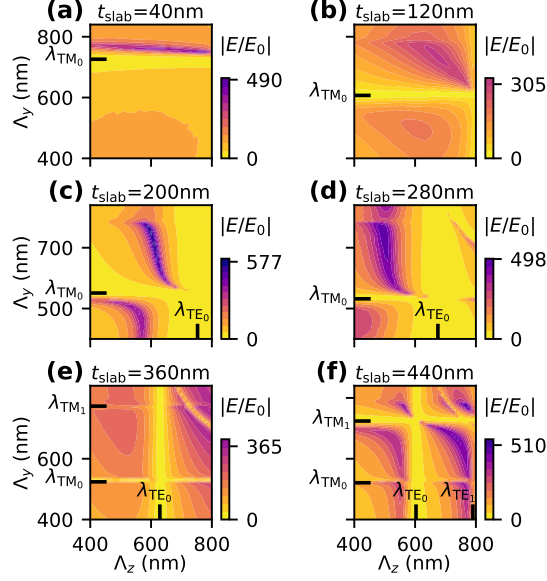


**Figure 4.** Near-field enhancement factor  $|E/E_0|$  as a function of periods  $\Lambda_y$  and  $\Lambda_z$  for several slab thicknesses  $t_{\text{slab}}$  obtained at the fixed wavelength  $\lambda_{\text{tg}} = 780$  nm. Thick black ticks with labels  $\lambda_{\text{TM}_0}$ ,  $\lambda_{\text{TM}_1}$ , and  $\lambda_{\text{TE}_0}$  mark the guided-mode wavelengths in the slab waveguide of the corresponding thickness.

counter-propagate along axis  $y$ . For higher-order empty-lattice TM modes with order  $n = 1$  (the blue dashed curve), another band gap is formed near the normalized frequency  $\omega/\omega_{\text{tg}} = 1.04$  at  $k_y = \pi/\Lambda_y$ .

If light is incident in the  $zx$ -plane and  $s$ -polarized, it couples effectively to the Bloch modes propagating in the  $z$ -direction. The excited LSPRs in the dimers still provide a high gap enhancement. In Fig. 3(d), one can observe the near-field enhancement spectra shown in band gaps near  $\omega/\omega_{\text{tg}} = 1.0$  and 1.08 due to the interaction of LSPRs with the  $\text{TM}_0^{(1,n)}$  modes at  $k_z = 0$  and  $k_z = \pi/\Lambda_z$ , respectively. The interaction leads to high near-field enhancement factors (see the dark regions in the figure). Additional empty-lattice TE and TM modes do not significantly affect the near-field enhancement and they are not shown in the figure.

#### 4. Near-field enhancement in a planar metasurface

We can now maximize the near-field enhancement by optimizing the periods  $\Lambda_y$  and  $\Lambda_z$ , as well as the slab thickness  $t_{\text{slab}}$ . As shown in Fig. 4(a-f), both the periods affect the near-field enhancement, and the fingerprints of band gaps are recognized as straight stripes of low near-field enhancement near the periods equal to the guided-mode wavelengths (indicated by thick black ticks with labels  $\lambda_{\text{TM}_0}$ ,  $\lambda_{\text{TM}_1}$ , and  $\lambda_{\text{TE}_0}$ ). The Bloch modes formed above or below the guided-mode wavelengths contribute the most to the near-field enhancement in the gaps of the nanoparticles. A maximum field enhancement,  $|E/E_0| = 577$ , is achieved at periods  $\Lambda_z = 595$  nm and  $\Lambda_y = 760$  nm for the

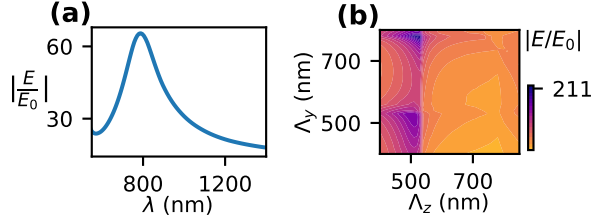


**Figure 5.** Near-field enhancement factors of (a) a single dimer as a function of wavelength  $\lambda$  and (b) a lattice of dimers on top of a semi-infinite silica as a function of periods  $\Lambda_y$  and  $\Lambda_z$ .

slab thickness  $t_{\text{slab}} = 200$  nm. Such a configuration allows for a SERS enhancement factor,  $\eta_{\text{SERS}}$ , of the order of  $10^{11}$  at a gap size of 6 nm. At smaller gaps, the enhancement factor is larger, but we consider 6 nm as a reasonable gap size that can be obtained in nanofabricated samples.

It is interesting to compare the near-field enhancement in the optimized metasurface to that of a single dimer and a lattice of dimers on a thick silica substrate. For an isolated single dimer on a thick substrate, the near field can be resonantly enhanced by a factor of 65 at  $\lambda = 780$  nm, as shown in Fig. 5(a). If such dimers are arranged periodically in a lattice on the same substrate, an extra factor of 3 can be obtained for the near-field enhancement [see Fig. 5(b)]. In our design, with a silver mirror positioned at a distance of 200 nm below the surface, an overall near-field enhancement of 577 is obtained. Hence, arranging the particles in a lattice on a slab waveguide resulted in about 80 times higher local-field intensity in the gaps compared to the case of isolated dimers on a thick substrate, providing an extra SERS enhancement of more than 6000 (calculated as a squared intensity enhancement). The presence of the waveguide additionally increases the local-field intensity by more than 7 times, corresponding to a 50-fold increase of  $\eta_{\text{SERS}}$ . It is well known that naked metal nanostructures of typical SERS substrates are not suitable for multiple use because of their fast and irreversible degradation caused, e.g., by humidity variations, surface oxidation, and contamination. The structures could be protected with a few-nm-thick dielectric coating, but this usually lowers  $\eta_{\text{SERS}}$  by orders of magnitude. The extra enhancement considered in this work can compensate for this decrease of SERS signal and allow making the substrates reusable.

We further explore the near-field enhancement spectra of three designed metasurfaces with  $t_{\text{slab}} = 200$  nm, marked by points D, E, and F in Fig. 6(a)-(c). For the metasurface at point D, the periods are  $\Lambda_y = 550$  nm and  $\Lambda_z = 595$  nm, and the near-field enhancement is very low due to the band gap near the normalized frequency  $\omega/\omega_{\text{tg}} = 1$  at  $k_y = 0$  [see Fig. 6(d)]. This band gap is formed because the period  $\Lambda_y$  matches with the modal wavelength  $\lambda_{\text{TM}_0} = 550$  nm of the fundamental TM mode propagating along the  $y$ -axis [see Fig. 2(a)].

At point E, the periods are  $\Lambda_y = 760$  nm and  $\Lambda_z = 755$  nm, with the latter being close to the modal wavelength  $\lambda_{\text{TE}_0} = 753$  nm of the fundamental TE mode propagating along the  $z$ -axis [see Fig. 2(a)]. This results in a band gap near the normalized frequency  $\omega/\omega_{\text{tg}} = 1$  at  $k_z = 0$  [see Fig. 6(e)], which makes the near-field enhancement low.

The maximum near-field enhancement is obtained for the metasurface at point F with a pair of periods  $\Lambda_y = 760$  nm and  $\Lambda_z = 595$  nm. As shown in Fig. 6(f), the upper band of the guided Bloch mode is formed at the normalized frequency  $\omega/\omega_{\text{tg}} = 1$  at  $k_y = 0$ , because  $\Lambda_y$  is larger than the

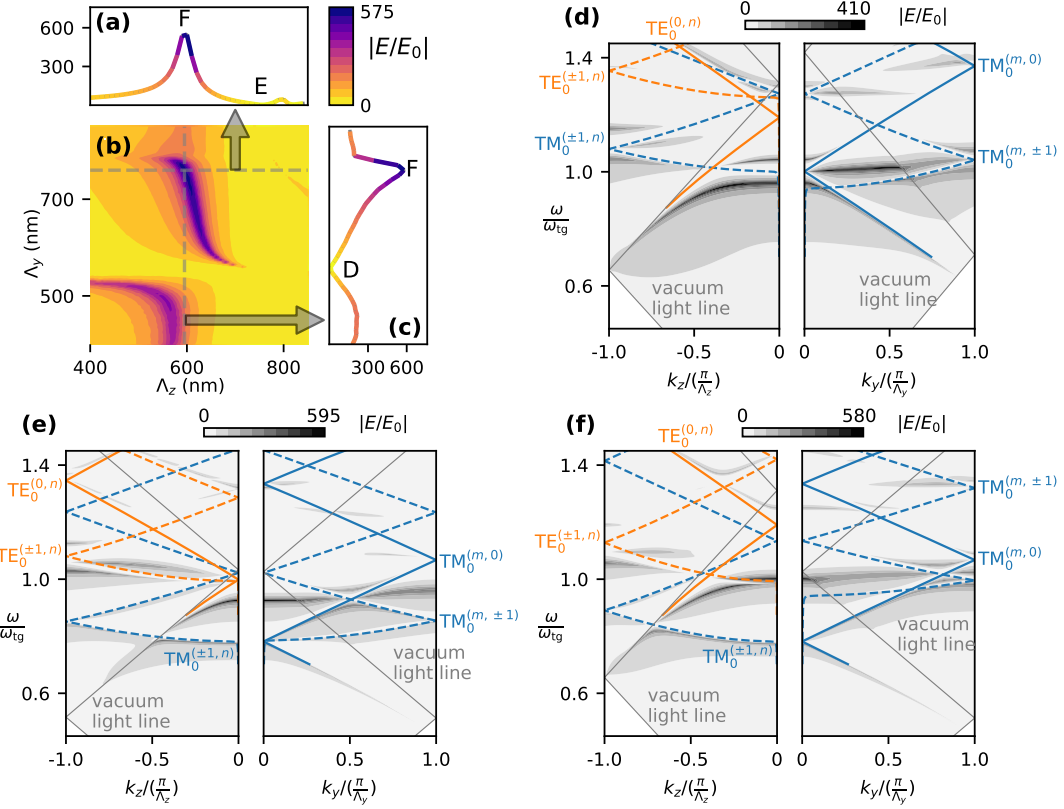


**Figure 6.** Near-field enhancement spectra for  $t_{\text{slab}} = 200$  nm and (a) a fixed period  $\Lambda_y = 760$  nm, (b) varying periods  $\Lambda_y$  and  $\Lambda_z$ , and (c) a fixed period  $\Lambda_z = 595$  nm. For three typical configurations at points D, E, and F, the near-field enhancement spectra as a function of the incidence angles along the  $y$  and  $z$  axes are shown in (d), (e), and (f), respectively. Blue and orange lines indicate the empty-lattice Bloch modes  $\text{TM}_0^{(m,n)}$  and  $\text{TE}_0^{(0,n)}$ , respectively. In both colours, solid lines indicate the zero-order modes, whereas the dashed lines stand for the 1st-order modes.

modal wavelength  $\lambda_{\text{TM}_0}$ . On the other hand, the lower band of the guided Bloch mode is formed at the normalized frequency  $\omega/\omega_{\text{tg}} = 1$  at  $k_z = 0$ , as  $\Lambda_z$  is smaller than the modal wavelength  $\lambda_{\text{TE}_0}$ . The upper and lower bands of the guided Bloch modes counter-propagating along the  $y$  and  $z$  axes jointly enhance the near-field in the gaps of the dimers.

## 5. Conclusions

We have shown that, with the aid of guided Bloch modes in a designed nonlocal optical metasurface, the local field intensity can be considerably increased in addition to the enhancement by isolated plasmonic nanoparticles. The additional enhancement mechanism relies on the coupling of the incident light to the LSPRs of individual nanoparticles and to the Bloch modes guided in a metal-dielectric slab waveguide beneath the particles. The coupling takes place at the second stop band

edge for normally incident light. The maximum enhancement is obtained by optimizing the two periods and the thickness of the waveguide. The approach clearly outperforms the lattice-resonance-based enhancement. For plasmonic nanodimers with a gap size of 6 nm, we obtained a SERS enhancement of  $10^{11}$ . By reducing the gap, the enhancement factor can be increased by further orders of magnitude. In addition, using dimers with sharp edges, such as bowtie antennae, would further enhance the local field intensity. We expect that the proposed mechanism of additional near-field enhancement will find applications not only in SERS, but also in fluorescence- and scattering-based plasmonic sensing, light-energy harvesting components, and nonlinear optics.

### Acknowledgments

We acknowledge the Academy of Finland Flagship Programme Photonics Research and Innovation (PREIN; grant No. 320167). We thank Dr. R. Kolkowski for fruitful discussions and advice on theoretical simulations of metasurfaces and slab waveguide modes. We also acknowledge the computational resources provided by the Aalto Science-IT project.

### References

- [1] Bo Liedberg, Claes Nylander, and Ingemar Lunström. Surface plasmon resonance for gas detection and biosensing. *Sensors and Actuators*, 4:299–304, January 1983. doi:10.1016/0250-6874(83)85036-7.
- [2] Jiří Homola, Sinclair S. Yee, and Günter Gauglitz. Surface plasmon resonance sensors: review. *Sensors and Actuators B: Chemical*, 54(1):3–15, January 1999. doi:10.1016/S0925-4005(98)00321-9.
- [3] Rupert F. Oulton, Volker J. Sorger, Thomas Zentgraf, Ren-Min Ma, Christopher Gladden, Lun Dai, Guy Bartal, and Xiang Zhang. Plasmon lasers at deep subwavelength scale. *Nature*, 461(7264):629–632, October 2009. doi:10.1038/nature08364.
- [4] Rupert F. Oulton. Surface plasmon lasers: sources of nanoscopic light. *Materials Today*, 15(1-2):26–34, January 2012. doi:10.1016/S1369-7021(12)70018-4.
- [5] Ke Liu, Ning Li, Devendra K. Sadana, and Volker J. Sorger. Integrated nanocavity plasmon light sources for on-chip optical interconnects. *ACS Photonics*, 3(2):233–242, February 2016. doi:10.1021/acspophotonics.5b00476.
- [6] Yin Liang, Chun Li, Yong-Zhen Huang, and Qing Zhang. Plasmonic nanolasers in on-chip light sources: prospects and challenges. *ACS Nano*, 14(11):14375–14390, November 2020. doi:10.1021/acsnano.0c07011.
- [7] D. M. Schaad, B. Feng, and E. T. Yu. Enhanced semiconductor optical absorption via surface plasmon excitation in metal nanoparticles. *Applied Physics Letters*, 86(6):063106, February 2005. doi:10.1063/1.1855423.
- [8] S. Pillai and M. A. Green. Plasmonics for photovoltaic applications. *Solar Energy Materials and Solar Cells*, 94(9):1481–1486, September 2010. doi:10.1016/j.solmat.2010.02.046.
- [9] Harry A. Atwater and Albert Polman. Plasmonics for improved photovoltaic devices. *Nature Materials*, 9(3):205–213, March 2010. doi:10.1038/nmat2629.
- [10] A. Bouhelier, M. Beversluis, A. Hartschuh, and L. Novotny. Near-field second-harmonic generation induced by local field enhancement. *Physical Review Letters*, 90(1):013903, January 2003. doi:10.1103/PhysRevLett.90.013903.

- [11] Johann Berthelot, Guillaume Bachelier, Mingxia Song, Padmnabh Rai, Gérard Colas des Francs, Alain Dereux, and Alexandre Bouhelier. Silencing and enhancement of second-harmonic generation in optical gap antennas. *Optics Express*, 20(10):10498–10508, May 2012. doi:10.1364/OE.20.010498.
- [12] Robert Czaplicki, Antti Kiviniemi, Mikko J. Huttunen, Xiaorun Zang, Timo Stolt, Ismo Vartiainen, Jérémie Butet, Markku Kuittinen, Olivier J. F. Martin, and Martti Kauranen. Less is more: Enhancement of second-harmonic generation from metasurfaces by reduced nanoparticle density. *Nano Letters*, 18(12):7709–7714, December 2018. doi:10.1021/acs.nanolett.8b03378.
- [13] T. Klar, M. Perner, S. Grosse, G. von Plessen, W. Spirk, and J. Feldmann. Surface-plasmon resonances in single metallic nanoparticles. *Physical Review Letters*, 80(19):4249–4252, May 1998. doi:10.1103/PhysRevLett.80.4249.
- [14] Stefan A. Maier. *Plasmonics: fundamentals and applications*. Springer, New York, 2007.
- [15] C. Ciraci, R. T. Hill, J. J. Mock, Y. Urzhumov, A. I. Fernández-Domínguez, S. A. Maier, J. B. Pendry, A. Chilkoti, and D. R. Smith. Probing the ultimate limits of plasmonic enhancement. *Science*, 337(6098):1072–1074, August 2012. doi:10.1126/science.1224823.
- [16] Encai Hao and George C. Schatz. Electromagnetic fields around silver nanoparticles and dimers. *The Journal of Chemical Physics*, 120(1):357, 2004. doi:10.1063/1.1629280.
- [17] Stephanie Dodson, Mohamed Haggui, Renaud Bachelot, Jérôme Plain, Shuzhou Li, and Qihua Xiong. Optimizing electromagnetic hotspots in plasmonic bowtie nanoantennae. *The Journal of Physical Chemistry Letters*, 4(3):496–501, February 2013. doi:10.1021/jz302018x.
- [18] Katrin Kneipp, Yang Wang, Harald Kneipp, Lev T. Perelman, Irving Itzkan, Ramachandra R. Dasari, and Michael S. Feld. Single molecule detection using surface-enhanced Raman scattering (SERS). *Physical Review Letters*, 78(9):1667–1670, March 1997. doi:10.1103/PhysRevLett.78.1667.
- [19] Shuming Nie and Steven R. Emory. Probing single molecules and single nanoparticles by surface-enhanced Raman scattering. *Science*, 275(5303):1102–1106, February 1997. doi:10.1126/science.275.5303.1102.
- [20] Amanda J. Haes, Christy L. Haynes, Adam D. McFarland, George C. Schatz, Richard P. Van Duyne, and Shengli Zou. Plasmonic materials for surface-enhanced sensing and spectroscopy. *MRS Bulletin*, 30(5):368–375, May 2005. doi:10.1557/mrs2005.100.
- [21] Younan Xia and Naomi J. Halas. Shape-controlled synthesis and surface plasmonic properties of metallic nanostructures. *MRS Bulletin*, 30(5):338–348, May 2005. doi:10.1557/mrs2005.96.
- [22] Arash Ahmadiivand, Burak Gerislioglu, Rajeev Ahuja, and Yogendra Kumar Mishra. Toroidal metaphotonics and metadevices. *Laser & Photonics Reviews*, 14(11):1900326, November 2020. doi:10.1002/lpor.201900326.
- [23] Martín Caldarola, Pablo Alabella, Emiliano Cortés, Mohsen Rahmani, Tyler Roschuk, Gustavo Grinblat, Rupert F. Oulton, Andrea V. Bragas, and Stefan A. Maier. Non-plasmonic nanoantennas for surface enhanced spectroscopies with ultra-low heat conversion. *Nature Communications*, 6(1):7915, August 2015. doi:10.1038/ncomms8915.
- [24] Arseniy I. Kuznetsov, Andrey E. Miroshnichenko, Mark L. Brongersma, Yuri S. Kivshar, and Boris Luk'yanchuk. Optically resonant dielectric nanostructures. *Science*, 354(6314):aag2472, November 2016. doi:10.1126/science.aag2472.

- [25] Ivano Alessandri and John R. Lombardi. Enhanced Raman scattering with dielectrics. *Chemical Reviews*, 116(24):14921–14981, December 2016. doi:10.1021/acs.chemrev.6b00365.
- [26] D. A. Weitz, S. Garoff, J. I. Gersten, and A. Nitzan. A comparison of Raman scattering, resonance Raman scattering, and fluorescence from molecules adsorbed on silver island films. *Journal of Electron Spectroscopy and Related Phenomena*, 29(1):363–370, January 1983. doi:10.1016/0368-2048(83)80089-9.
- [27] Arash Ahmadvand, Michael Semmlinger, Liangliang Dong, Burak Gerislioglu, Peter Nordlander, and Naomi J. Halas. Toroidal dipole-enhanced third harmonic generation of deep ultraviolet light using plasmonic meta-atoms. *Nano Letters*, 19(1):605–611, January 2019. doi:10.1021/acs.nanolett.8b04798.
- [28] F. Javier García de Abajo. Nonlocal effects in the plasmons of strongly interacting nanoparticles, dimers, and waveguides. *The Journal of Physical Chemistry C*, 112(46):17983–17987, November 2008. doi:10.1021/jp807345h.
- [29] Ruben Esteban, Andrei G. Borisov, Peter Nordlander, and Javier Aizpurua. Bridging quantum and classical plasmonics with a quantum-corrected model. *Nature Communications*, 3(1):825, May 2012. doi:10.1038/ncomms1806.
- [30] Yu Luo, A. I. Fernandez-Dominguez, Aeneas Wiener, Stefan A. Maier, and J. B. Pendry. Surface plasmons and nonlocality: a simple model. *Physical Review Letters*, 111(9), August 2013. doi:10.1103/PhysRevLett.111.093901.
- [31] Wenqi Zhu and Kenneth B. Crozier. Quantum mechanical limit to plasmonic enhancement as observed by surface-enhanced Raman scattering. *Nature Communications*, 5:5228, October 2014. doi:10.1038/ncomms6228.
- [32] Christian Girard, Aurélien Cuche, Erik Dujardin, Arnaud Arbouet, and Adnen Mlayah. Molecular decay rate near nonlocal plasmonic particles. *Optics Letters*, 40(9):2116–2119, May 2015. doi:10.1364/OL.40.002116.
- [33] Wenqi Zhu, Ruben Esteban, Andrei G. Borisov, Jeremy J. Baumberg, Peter Nordlander, Henri J. Lezec, Javier Aizpurua, and Kenneth B. Crozier. Quantum mechanical effects in plasmonic structures with subnanometre gaps. *Nature Communications*, 7(1):11495, June 2016. doi:10.1038/ncomms11495.
- [34] Zhiwen Shi, Xiaoping Hong, Hans A. Bechtel, Bo Zeng, Michael C. Martin, Kenji Watanabe, Takashi Taniguchi, Yuen-Ron Shen, and Feng Wang. Observation of a Luttinger-liquid plasmon in metallic single-walled carbon nanotubes. *Nature Photonics*, 9(8):515–519, August 2015. doi:10.1038/nphoton.2015.123.
- [35] G. Vecchi, V. Giannini, and J. Gómez Rivas. Shaping the fluorescent emission by lattice resonances in plasmonic crystals of nanoantennas. *Physical Review Letters*, 102(14), April 2009. doi:10.1103/PhysRevLett.102.146807.
- [36] S. R. K. Rodriguez, A. Abass, B. Maes, O. T. A. Janssen, G. Vecchi, and J. Gómez Rivas. Coupling bright and dark plasmonic lattice resonances. *Physical Review X*, 1(2), December 2011. doi:10.1103/PhysRevX.1.021019.
- [37] Danqing Wang, Ankun Yang, Weijia Wang, Yi Hua, Richard D. Schaller, George C. Schatz, and Teri W. Odom. Band-edge engineering for controlled multi-modal nanolasing in plasmonic superlattices. *Nature Nanotechnology*, 12(9):889–894, September 2017. doi:10.1038/nnano.2017.126.

- [38] V. G. Kravets, A. V. Kabashin, W. L. Barnes, and A. N. Grigorenko. Plasmonic surface lattice resonances: a review of properties and applications. *Chemical Reviews*, 118(12):5912–5951, June 2018. doi:10.1021/acs.chemrev.8b00243.
- [39] Weijia Wang, Mohammad Ramezani, Aaro I. Väkeväinen, Päivi Törmä, Jaime Gómez Rivas, and Teri W. Odom. The rich photonic world of plasmonic nanoparticle arrays. *Materials Today*, 21(3):303–314, April 2018. doi:10.1016/j.matod.2017.09.002.
- [40] Charles Cherqui, Marc R. Bourgeois, Danqing Wang, and George C. Schatz. Plasmonic surface lattice resonances: Theory and computation. *Accounts of Chemical Research*, 52(9):2548–2558, September 2019. doi:10.1021/acs.accounts.9b00312.
- [41] F. J. García de Abajo. Colloquium: Light scattering by particle and hole arrays. *Reviews of Modern Physics*, 79(4):1267–1290, October 2007. doi:10.1103/RevModPhys.79.1267.
- [42] Per Lunnemann and A. Femius Koenderink. Dispersion of guided modes in two-dimensional split ring lattices. *Physical Review B*, 90(24):245416, December 2014. doi:10.1103/PhysRevB.90.245416.
- [43] Anton D. Utyushev, Vadim I. Zakomirnyi, and Ilia L. Rasskazov. Collective lattice resonances: Plasmonics and beyond. *Reviews in Physics*, 6:100051, June 2021. doi:10.1016/j.revip.2021.100051.
- [44] Shengli Zou, Nicolas Janel, and George C. Schatz. Silver nanoparticle array structures that produce remarkably narrow plasmon lineshapes. *The Journal of Chemical Physics*, 120(23):10871, 2004. doi:10.1063/1.1760740.
- [45] Michael B. Ross, Chad A. Mirkin, and George C. Schatz. Optical properties of one-, two-, and three-dimensional arrays of plasmonic nanostructures. *The Journal of Physical Chemistry C*, 120(2):816–830, January 2016. doi:10.1021/acs.jpcc.5b10800.
- [46] Frédéric Laux, Nicolas Bonod, and Davy Gérard. Single emitter fluorescence enhancement with surface lattice resonances. *The Journal of Physical Chemistry C*, 121(24):13280–13289, June 2017. doi:10.1021/acs.jpcc.7b04207.
- [47] Fei Ding, Yuanqing Yang, Rucha A. Deshpande, and Sergey I. Bozhevolnyi. A review of gap-surface plasmon metasurfaces: fundamentals and applications. *Nanophotonics*, 7(6):1129–1156, June 2018. doi:10.1515/nanoph-2017-0125.
- [48] A. Christ, S. G. Tikhodeev, N. A. Gippius, J. Kuhl, and H. Giessen. Waveguide-plasmon polaritons: strong coupling of photonic and electronic resonances in a metallic photonic crystal slab. *Physical Review Letters*, 91(18):183901, October 2003. doi:10.1103/PhysRevLett.91.183901.
- [49] S. R. K. Rodriguez, S. Murai, M. A. Verschuuren, and J. Gómez Rivas. Light-emitting waveguide-plasmon polaritons. *Physical Review Letters*, 109(16):166803, October 2012. doi:10.1103/PhysRevLett.109.166803.
- [50] O. Y. Yermakov, A. I. Ovcharenko, M. Song, A. A. Bogdanov, I. V. Iorsh, and Yu. S. Kivshar. Hybrid waves localized at hyperbolic metasurfaces. *Physical Review B*, 91(23):235423, June 2015. doi:10.1103/PhysRevB.91.235423.
- [51] Radoslaw Kolkowski and Andriy Shevchenko. Enabling infinite  $Q$  factors in absorbing optical systems. *Nanophotonics*, 12(17):3443–3454, August 2023. doi:10.1515/nanoph-2023-0281.
- [52] Adam Overvig and Andrea Alù. Diffractive nonlocal metasurfaces. *Laser & Photonics Reviews*, 16(8):2100633, 2022. doi:10.1002/lpor.202100633.

- [53] Andriy Shevchenko, Victor Ovchinnikov, and Anna Shevchenko. Large-area nanostructured substrates for surface enhanced Raman spectroscopy. *Applied Physics Letters*, 100(17):171913, April 2012. doi:10.1063/1.4707158.
- [54] K. T. Carron, W. Fluhr, M. Meier, A. Wokaun, and H. W. Lehmann. Resonances of two-dimensional particle gratings in surface-enhanced Raman scattering. *Journal of the Optical Society of America B*, 3(3):430–440, March 1986. doi:10.1364/JOSAB.3.000430.
- [55] S. G. Tikhodeev, A. L. Yablonskii, E. A. Muljarov, N. A. Gippius, and Teruya Ishihara. Quasiguided modes and optical properties of photonic crystal slabs. *Physical Review B*, 66(4):045102, July 2002. doi:10.1103/PhysRevB.66.045102.
- [56] Mikhail Polyanskiy. refractiveindex.info database, 2008.
- [57] P. B. Johnson and R. W. Christy. Optical constants of the noble metals. *Physical Review B*, 6(12):4370–4379, 1972. doi:10.1103/PhysRevB.6.4370.
- [58] Introduction to COMSOL Multiphysics® v. 6.0. *COMSOL AB, Stockholm, Sweden*, 2022. URL: [www.comsol.com](http://www.comsol.com).
- [59] Netgen/ngsolve is a high performance multiphysics finite element software. it is widely used to analyze models from solid mechanics, fluid dynamics and electromagnetics. due to its flexible python interface new physical equations and solution algorithms can be implemented easily. URL: [ngsolve.org](http://ngsolve.org).
- [60] Z.S. Sacks, D.M. Kingsland, R. Lee, and Jin-Fa Lee. A perfectly matched anisotropic absorber for use as an absorbing boundary condition. *IEEE Transactions on Antennas and Propagation*, 43(12):1460–1463, Dec./1995. doi:10.1109/8.477075.
- [61] Stephen D. Gedney. *Introduction to the finite-difference time-domain (FDTD) method for electromagnetics*. Synthesis Lectures on Computational Electromagnetics. Springer International Publishing, Cham, 2011. doi:10.1007/978-3-031-01712-4.
- [62] L. Solymar and E. Shamonina. *Waves in metamaterials*. Oxford University Press, Oxford ; New York, 2009.
- [63] V. Yannopapas and N. Stefanou. Optical excitation of coupled waveguide-particle plasmon modes: A theoretical analysis. *Physical Review B*, 69(1):012408, January 2004. doi:10.1103/PhysRevB.69.012408.
- [64] Dmitry Khlopin, Frédéric Laux, William P. Wardley, Jérôme Martin, Gregory A. Wurtz, Jérôme Plain, Nicolas Bonod, Anatoly V. Zayats, Wayne Dickson, and Davy Gérard. Lattice modes and plasmonic linewidth engineering in gold and aluminum nanoparticle arrays. *Journal of the Optical Society of America B*, 34(3):691–700, March 2017. doi:10.1364/JOSAB.34.000691.